# Role of Atomic Relaxation in Hydrogen-Induced Amorphization

M. Katagiri and H. Onodera

National Institute for Materials Science
1-2-1 Sengen, Tsukuba, Ibaraki 305-0047, Japan

## ABSTRACT

The microscopic mechanism of Hydrogen-Induced Amorphization (HIA) in C15 Laves phases of $AB_2$ compounds is studied. Experimentally, compounds in which the AA internuclear distance is reduced and BB internuclear distance expanded compared to pure crystals show Hydrogen-Induced Amorphization which suggests that the relative atomic size is the controlling factor. We investigate the role of the size effect by static and Molecular Dynamics methods using Lennard-Jones potentials. Our simulations show that in such a compound, the bulk modulus is remarkably reduced by hydrogenation compared to the isotropic tensile load, so that elastic instability is facilitated. This situation is caused by the negative increase of the pressure-fluctuation contribution in the elastic constant. We also report the fracture process under isotropic tensile loading. An elastic analysis at sublattice level shows that one of the sublattices is less stable in the HIA material.

## KEYWORDS

molecular dynamics, hydrogen, Laves phase, fracture, amorphous, softening, elastic instability

## INTRODUCTION

Hydrogen-Induced Amorphization (HIA) is a phase transformation from crystalline to amorphous induced by hydrogenation. HIA is a potential method for preparing amorphous alloys since hydrogenation and dehydrogenation can be done easily and rapidly. In addition, HIA has a close relation with the structural change of hydrogen-storage alloys which determines their performance [1]. For effective materials design using HIA, it is important to understand the atomistic mechanism of this process. For this purpose, computer simulation is a powerful tool.

Aoki et al [2] studied HIA of C15 Laves phase $AB_2$ compounds experimentally. They found that the relative atomic size is the controlling factor of the occurrence of HIA. HIA does not occur when the ratio of the Goldschmidt radii of A and B atoms, $R_A/R_B$, is less than 1.37 (A = rare earth, B = Al). In this ratio, the internuclear distances between both AA and BB atoms contract compared to those in the pure crystals [2]. On the other hand, HIA occurs when the ratio is larger than 1.37 (A = rare earth, B = Fe, Co, Ni). In this ratio, the AA internuclear distance contracts and BB internuclear distance expands. Thus it is known that the size effect is essential. Our goal is to reveal the role of the size effect at the trigger of HIA [3, 4, 5].

## METHOD

*Model*

$YAl_2$ and $CeNi_2$ were modeled. $YAl_2$ is a non-HIA material and $CeNi_2$ is a HIA material. We used pair-wise Lennard-Jones (L-J) 12-6 potential to reveal the size effect. For different species pairs, the

geometric combination rule was used. As for hydrogen, only repulsion was taken into account [4]. By the analysis of the equation of state using our potential, it is known that *both the YY and AlAl internuclear distances contract in $YAl_2$, while CeCe internuclear distance contracts and NiNi internuclear distance expands in $CeNi_2$*. This corresponds to experimental results reported by Aoki et al. [2]. The ratio $R_Y/R_{Al}$ is 1.27 and $R_{Ce}/R_{Ni}$ is 1.46 in our model. Details of the interatomic potentials are in a reference [2]. The total number of metal atoms in the simulation cell is 192 with three-dimensional periodic boundary condition. We compared non-hydrogenated systems under isotropic tensile load and hydrogenated systems at zero pressure.

*Elastic Stability*

We treat homogeneous systems which do not contain any surface or defect. The dynamical stability of homogeneous lattice can be discussed by elastic stability criteria [6]. We calculated elastic constants $C^{ijkl}$ by fluctuation formula [7] from microcanonical molecular dynamics data.

$$C^{ijkl} = -\frac{\Omega_0}{kT}\delta(P^{ij}P^{kl}) + \frac{2MkT}{\Omega_0}(\delta^{il}\delta^{jk} + \delta^{ik}\delta^{jl}) + \frac{1}{\Omega_0} < \sum_a \sum_{b(>a)} (\frac{u'' - u'/r_{ab}}{r_{ab}^2}) r_{ab}^i r_{ab}^j r_{ab}^k r_{ab}^l > \qquad (1)$$

Each term shows the pressure-fluctuation, kinetic and potential contributions, respectively. $\Omega_0$ is the total volume, $T$ the temperature, $k$ the Boltzmann factor and $M$ the number of the metal atoms. The superscripts $i$, $j$, $k$ and $l$ are the Cartesian indices. $P^{ij}$ is the pressure tensor, $<>$ the ensemble average and $\delta(P^{ij}P^{kl})$ the ensemble fluctuation. Note that the summations are taken over the metal atoms excluding hydrogen. By using the elastic constants obtained here, we calculated the elastic stability criteria for cubic symmetry at external pressure $P$ [6].

$$B = \frac{1}{3}(C_{11} + 2C_{12} + P) \qquad (2)$$

$$G' = \frac{1}{2}(C_{11} - C_{12} - 2P) \qquad (3)$$

$$G = 4(C_{44} - P) \qquad (4)$$

Here, $P < 0$ for tension. All are finite and positive so that the crystal lattice is elastically stable [6]. The vanishing of the bulk-modulus $B$ is the instability of lattice decohesion by pure dilation with no symmetry change. The vanishing of the tetragonal shear-modulus $G'$ leads to symmetry breaking (bifurcation) with volume conservation. The vanishing of the rhombohedral shear-modulus $G$ gives a simple shear instability along one of the symmetry directions with volume conservation [6].

## ELASTIC INSTABILITY BY ISOTROPIC TENSILE LOAD

*Molecular Dynamics*

Figure 1 shows snapshots of the fracture for *non-hydrogenated* $YAl_2$ and $CeNi_2$ caused by an isotropic tensile load at temperature $T_s = 0.05$ and 0.06, respectively. Here the temperature is scaled by the melting one calculated by MD simulation [4]. $YAl_2$ shows a kind of cleavage by decohesion with maintaining the local lattice structure. On the other hand, $CeNi_2$ shows amorphous-like structure. By examining snapshots during the amorphization process it can be seen that the trigger of the amorphization is the movement of Ni atoms rather than Ce, as also seen in the HIA modeled by the embedded-atom potential [3]. A discontinuous potential-energy decrease is observed [4].

*Static Calculations*

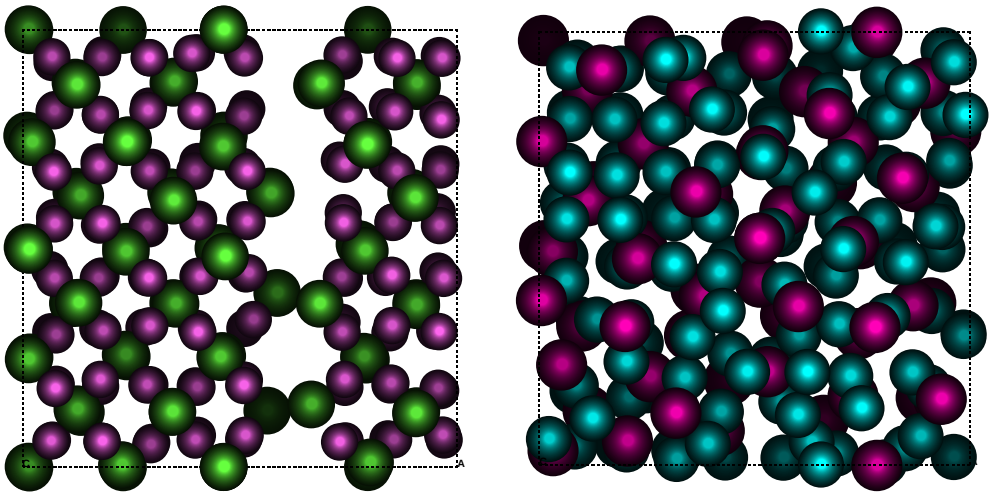

**Figure 1**: MD result of the fracture by isotropic tensile load. $YAl_2$ (left) shows cleavage fracture, while $CeNi_2$ (right) is collapsed to a amorphous-like structure.

We discuss the origin of the different fracture mode described above on the basis of the elastic stability criteria. For this purpose, we extend the definition of elastic constant of total lattice to the sublattice level. We define the potential part of the elastic constant of a sublattice as follows.

$$C^{ijkl}_{sub} = \frac{1}{\Omega_0} < \sum_{a \in sub} \sum_{b \neq a} \frac{1}{2} (\frac{u'' - u'/r_{ab}}{r^2_{ab}}) r^i_{ab} r^j_{ab} r^k_{ab} r^l_{ab} > . \tag{5}$$

Here *sub* means sublattice. Similar to the criteria for total lattice, the definitions are extended to sublattice level. Note that the sublattice also has cubic symmetry. Here, we consider only the potential contribution in the definitions. It is approximately valid for non-hydrogenated systems under the isotropic load, because the reduction of potential part in elastic constants contributes mainly in the elastic unstabilization of homogeneous lattice by the load.

$$B_{sub} = \frac{1}{3}(C_{11,sub} + 2C_{12,sub} + P_{sub}) \tag{6}$$

$$G'_{sub} = \frac{1}{2}(C_{11,sub} - C_{12,sub} - 2P_{sub}) \tag{7}$$

$$G_{sub} = 4(C_{44,sub} - P_{sub}) \tag{8}$$

Figure 2 shows the bulk-modulus stability under an isotropic load. In each simulation the simulation cell was expanded by rescaling the atomic positions. Figure 2(a) shows the stability change of $YAl_2$. The bulk moduli of total and sublattices become zero at almost the same cell length of 1.66nm, which means that the sublattice-instability points agree well with the instability point of the total lattice. The critical cell-length predicted by the instability point of total lattice is in good agreement with that obtained by MD simulations at low temperatures. Figure 2(b) shows the stability change of $CeNi_2$ at T=0K for homogeneous rescaling. The bulk modulus of the Ni sublattice becomes zero at about 1.50nm cell length. The total-lattice instability has not been reached at this length. However this critical cell-length of the Ni sublattice is in good agreement with the onset of amorphization seen in the MD simulations. Thus it seems that the instability of the Ni sublattice is the trigger for amorphization.

The different modes of fracture seen in the two MD simulations can be interpreted by such elastic stability argument. $YAl_2$ is fractured by the decohesion of the total lattice, since the instabilities of total and sublattice are realized together. When a cleavage fracture occurs at a local part of lattice by thermal fluctuation, it propagates to the whole region. On the other hand, for $CeNi_2$, the sublattice of Ni atoms becomes unstable, leading to amorphization. The instability of the Ni sublattice is associated with the expansion of the Ni-Ni distance in the Laves phase.

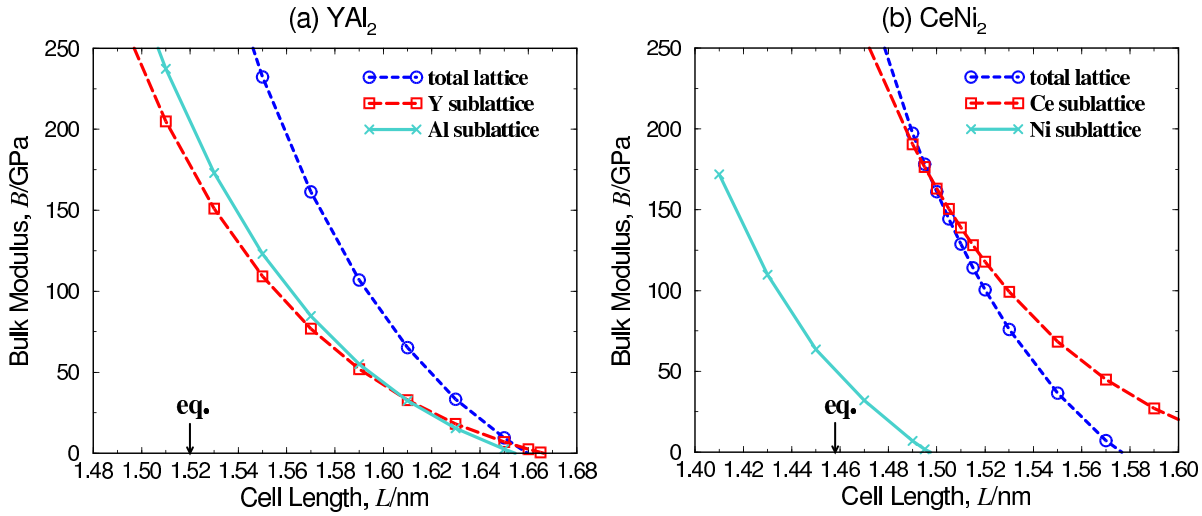


**Figure 2**: Static calculations of bulk-modulus stability at sublattice level under isotropic tensile load.

Note that shear-modulus $G'$ and $G$-instabilities are not reached before the lattice instability for both $YAl_2$ and $CeNi_2$. In both cases, the bulk-modulus instability governs the fracture.

*Equation of State*
We have illustrated the fracture mode of $YAl_2$ and $CeNi_2$. To address the behavior for a general combination of atomic sizes, we calculated the inter-atomic contraction/expansion and the critical cell length at which the bulk modulus instability occurs, as shown in Figure 3. It was calculated by constructing the equation of state within the third neighbor interaction shell. In Figure 3(a), the negative (positive) value of $(r-R)/R$ means the atomic contraction (expansion). At 1.225, there is a contraction of both A and B interatomic distances giving geometrical ideal lattice. The lower and upper limits of the size ratio for sublattice stabilities at zero pressure are given by 1.01 and 1.55, respectively. In fact, all materials reported in a reference [2] exist in this range. The ratio of 1.225 gives the equivalent critical length of A and B-sublattices. Note that hard sphere model gives the ideal lattice at the ratio of 1.225. In the range of $1.225 < R_A/R_B < 1.33$, both A and B interatomic distances contract. The stability of the B-sublattice is lower than that of the A-sublattice. In the range of $1.33 < R_A/R_B$, A distances contract and B distances expand. The stability of B-sublattice is considerably lower than that of A-sublattice.

## ELASTIC INSTABILITY BY HYDROGENATION

We consider the elastic response of the lattice to hydrogenation. Figure 4 shows the elastic stability of (a) $YAl_2$ and (b) $CeNi_2$ under hydrogenation at zero pressure. In the figure, $\times$ denotes the bulk-modulus $B$-stability in Eqn.2 and $+$ denotes the shear-modulus $G'$-stability in Eqn.3. For comparison, $B$ and $G'$-stabilities of non-hydrogenated systems under isotropic tensile load are also shown by $\bigcirc$ and $\square$, respectively. In $CeNi_2$, the bulk-modulus $B$ is reduced by hydrogenation (denoted by $\times$), leading to a lattice instability: Unlike $B$, $G'$ does not soften. The elastic constants $C_{11}$ and $C_{12}$ decrease with hydrogenation, but for $G'$ which is the difference between $C_{11}$ and $C_{12}$ (Eqn.3), the softenings are canceled. In $YAl_2$, we did not observe any evidence of such a softening effect. We found that hydrogenation and isotropic tensile loading gave similar elastic stability changes. This suggests that hydrogenation simply causes a volume expansion, and the softening due to the volume expansion is observed. On the other hand, the softening by hydrogenation in $CeNi_2$ is caused by the negative increase of the pressure-fluctuation term in the elastic constant. The softening in a simple volume expansion of $CeNi_2$ is caused by the decrease of the potential term in the elastic constant as in Eqn.1. Such a softening by volume expansion needs a large expansion to reach the elastic instability for amorphization. However, amorphization by hydrogenation occurs at a lower volume. The reason for the reduction in

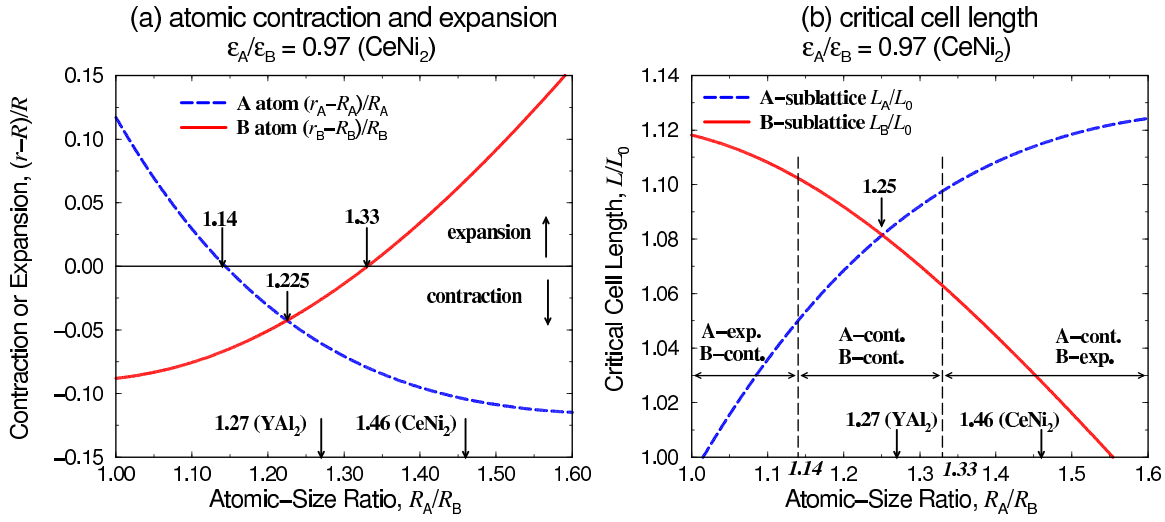


**Figure 3**: (a) Atomic contraction/expansion and (b) the critical cell length at the bulk modulus instability by the isotropic tensile load. $\epsilon$ is the Lennard-Jones energy parameter. $R$ is the Goldschmidt radius of pure crystal state estimated by our potential. $r$ is the radius in Laves phase. $L_0$ is the equilibrium cell length at zero pressure. The ratio of energy parameters $\epsilon$ is adjusted for $CeNi_2$ while that of the size parameters are varied.

the pressure-fluctuation term is that metal atoms in the neighborhood of hydrogen deviate locally from their equilibrium positions. Even if such a relaxation is energetically small, the change in the pressure fluctuations is large.

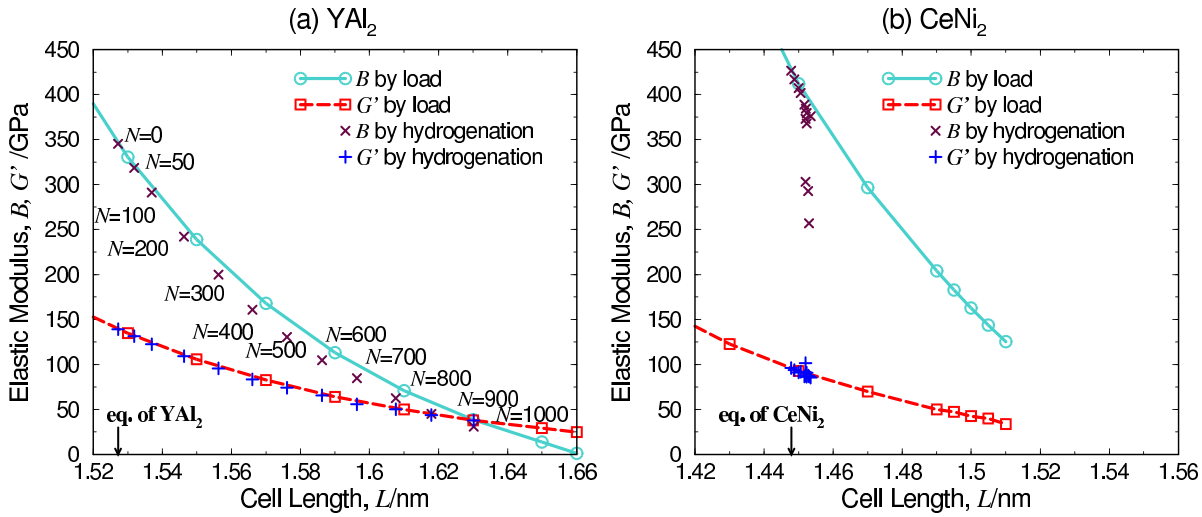


**Figure 4**: Elastic stability under isotropic tensile loading or by hydrogenation. $N$ is the number of hydrogen atoms incorporated into $A_{64}B_{128}$ systems. As for $CeNi_2$, $N < 37$.

## CONCLUSIONS

Hydrogen-Induced Amorphization (HIA) was simulated by static and molecular dynamics (MD) methods. We compared non-HIA and HIA materials, $YAl_2$ and $CeNi_2$, respectively. The changes of the elastic stability by the isotropic tensile load and the hydrogenation were calculated.

The fracture process of non-hydrogenated systems by isotropic tensile load was simulated by MD. The lattice fractured at the cell length where the bulk modulus falls to zero. In $YAl_2$, the bulk moduli of total lattice and sublattices fall to zero at a similar volume, and a cleavage surface is created. On the other hand, in $CeNi_2$, the bulk modulus of Ni sublattice is relatively small and falls to zero first. The

amorphous-like structure is obtained. Such a difference in the mode of fracture is caused by the size effect. Compared to the pure states, Y and Al internuclear distances contract, while Ce internuclear distances contract and Ni internuclear distances expand in Laves phase. In $CeNi_2$, the bulk-modulus stability of Ni sublattice is low due to the expansion of the internuclear distances and falls to zero first.

We incorporated hydrogen into the systems. $YAl_2$ did not show HIA. On the other hand, once the amount of hydrogen atoms exceeds a critical value, $CeNi_2$ showed HIA [4]. In $YAl_2$, hydrogenation simply increases the volume and the bulk modulus is reduced because of the non-linearity of the interatomic potentials. A similar reduction is observed under an isotropic tensile load. The main cause of the reduction is the potential term in the elastic constant. On the other hand, in $CeNi_2$, hydrogenation greatly reduces the bulk modulus. This reduction is mainly caused by the negative increase of the pressure-fluctuation term in the elastic constant. As a result, hydrogenation lead to the amorphization at a much smaller volume than under a load. The increase of the pressure-fluctuation is the result of the atomic relaxation induced by hydrogenation. In $CeNi_2$, the contraction and expansion are realized simultaneously, and relaxation can occur by hydrogenation. Even if the potential-energy change resulting from the relaxation is small, the change in pressure fluctuation is high.

These features can also be understood by the consideration of the equation of state for these compounds. When the size ratio exceeds 1.33, the bulk-modulus stability of the sublattice of B-atoms becomes low compared to that of A-atoms. However, there is no evidence that the ratio of 1.33 gives the critical ratio for HIA. The stability changes continuously as the ratio increases. This suggests that the mechanism of HIA cannot be understood by simple volume expansion and the atomic relaxations play an important role in it. When the internuclear distances of one sublattice expand and the other contract relative to pure crystals, relaxation occurs.

It is concluded that the role of the size effect in HIA is to allow the atomic relaxation on hydrogenation and to facilitate the elastic instability by the increase of pressure fluctuations.

*Acknowledgement*
We acknowledge Profs. Ruth Lynden-Bell at Queen's University of Belfast and Ali Alavi at University of Cambridge. Calculations were performed on Numerical Materials Simulator at NIMS.

## REFERENCES

[1] Aoki, K. and Masumoto, K. (1995) *Materia Japan* **34**, 126.

[2] Aoki, K., Li, X. G. and Masumoto, T. (1992) *Acta Metall. Mater.* **40**, 1717.

[3] Katagiri, K. and Onodera, H. (1999) *Trans. MRS-J* **24**, 245.

[4] Katagiri, M. and Onodera, H. (1999) *Mater. Trans., JIM* **40**, 1274.

[5] Katagiri, M. and Onodera, H. (2001) *J. Phase Equilibria in press.*

[6] Wang, J., Li, J., Yip, S., Phillpot, S. and Wolf, D. (1995) *Phys. Rev.* **B 52**, 12627.

[7] Ray, J. R., Moody, M. C. and Rahman, A. (1985) *Phys. Rev.* **B 32**, 733.